OFDM-based Dual Function Communications-Radar Utilizing the 4D Modified Matrix Pencil Method

Samuel P. Lavery, Navneet Garg and Tharmalingam Ratnarajah
Institute for Digital Communications, The University of Edinburgh, Edinburgh, Scotland

***Abstract*—Increased competition between wireless communications and radar systems motivates the use of dual-function communications-radar (DFRC) devices, which perform both functions simultaneously. Orthogonal frequency-division multiplexing (OFDM) waveforms that echo from targets can be compared with the transmitted waveform to isolate phase-shifts related to targets' ranges, velocities, azimuth angles and elevation angles. Extending the modified matrix enhancement matrix pencil method (MMEMP) to four dimensions (4D), this paper estimates the target parameters, comparing estimates to the Cramér-Rao lower bound (CRLB). A Fifth Generation New Radio-compliant (5G NR) system is simulated, demonstrating superior precision to Fourier- and MUSIC-based parameter estimation.**

I. Introduction

Congestion of the radio frequency (RF) spectrum results from proliferation of wireless communications [1] and radar systems, aiming to meet demands for high-speed data transfer and remote sensing, respectively. Competition lowers bit rates in communications and reduces probability of detection in radar systems. To reduce interference, dual-function communications-radar (DFCR) systems utilize one waveform to perform both operations simultaneously [2]–[4]. A singular DFCR base-station (DFBS) can achieve lower cost, space, weight and power requirements than two independent systems.

Orthogonal frequency-division multiplexing (OFDM) communications waveforms are suitable for DFBSs [5], [6]. Echoes from targets in the environment can be compared with the transmitted waveform, isolating phase-shifts related to and allowing estimation of ranges and velocities of those targets. Phase shifts of the received signal across an antenna array allow for azimuth and elevation angle estimation.

Matrix pencil (MP) techniques estimate the frequencies from sums of complex (damped) sinusoids [7]. Application of the one-dimensional (1D) technique has been used in estimation of angles of arrival (AoA) for a massive antenna array [8] and pole extraction from underwater targets [9]. Signal AoA and times of arrival have been estimated with 2D MP techniques [10], [11], which has also been used for imaging [12]. Using 3D MP, azimuth and elevation AoA have been estimated simultaneously with signal frequency [13].

This work was supported by the UK Engineering and Physical Sciences Research Council (EPSRC), the University of Edinburgh and Leonardo MW through the CASE Studentship Scheme.

979-8-3503-3959-8/23/$31.00 ©2023 IEEE

One method is the 2D matrix enhancement matrix pencil (MEMP) technique [14] which takes a moving window through data to enhance it, then extracts the normalized frequencies. It is an 'off-grid' method: accuracy is limited by the signal-to-noise ratio (SNR). The 2D modified MEMP (MMEMP) technique [15] improves computational efficiency and bypasses an error the MEMP technique is susceptible to. It has been extended to 3D to perform AoA estimation [16].

Our previous works [17], [18] applied Fourier transforms and the MUSIC algorithm [19] to estimate target range, velocity, azimuth angle and elevation angles from an airborne DFBS. These methods are 'on-grid': accuracy is limited by resolution of the search space. Here we extend the MMEMP technique to estimate target parameters in a 4D parameter space and present results from Monte-Carlo simulations.

II. System Model

The scene contains one DFBS, K point targets and user equipment which may receive downlink communications. Relative to the DFBS, the kth point target has range, velocity, azimuth angle and elevation angle parameters $\mathbf{w}_k = [R_k, v_k, \theta_k, \phi_k]$. Signal echoes undergo Doppler shift $f_{D,k} = 2v_k f_c/c$ with signal carrier frequency f_c and speed of light c.

OFDM waveforms transmit N_{ca} data subcarriers simultaneously for each of N_{sym} OFDM symbols. M-quadrature amplitude modulation (QAM) encodes binary data into the symbols. For the ηth subcarrier and μth OFDM time slot, data symbol $d_{Tx}(\eta, \mu)$ is embedded into the signal via an inverse discrete Fourier transform (DFT) [20]. Each OFDM symbol conveys $N_{ca} \times \log_2(M)$ bits of information.

Subcarriers have spacing Δf Hz, the ηth subcarrier having frequency $f_\eta = \eta\Delta f$ Hz, and the signal bandwidth is $BW = N_{ca}\Delta f$ Hz. Inter-carrier interference arises due to Doppler shifts in echoes from moving targets, but subcarrier orthogonality is ensured by limiting $10 f_{D,k} < \Delta f \;\forall\; k$ [6].

An OFDM symbol has period T_{sym} s, comprising a data signal preceded by a guard period T_{cyc} s, which limits inter-symbol interference from multipath effects. Here we assume no multipath, but by limiting spread in target range, echoes from different targets arrive in the same OFDM time slots, i.e., delay between target signals is less than the guard period, $2(\max_k R_k - \min_k R_k)/c < T_{cyc}$. We also assume the system doesn't suffer from self-interference, achievable in full-duplex systems with cancellation methods [21]–[23]. Finally, the transmitted symbols and received echoes are assumed to have negligible time-frequency mismatch [24].

Signals are transmitted and received by the square uniform planar array (UPA) on the DFBS, with N_{BS}-by-N_{BS} isotropic antennas in the $y-z$ plane. Antennas use phased array beamforming with normalized steering vector $\mathbf{a}(\theta,\phi) \in \mathbb{C}^{N_{BS}^2 \times 1}$ for AoA (θ,ϕ), with θ the azimuth angle and ϕ the elevation angle. In the pth row and qth column of the UPA [25]

$$a(\theta,\phi;p,q) = \frac{1}{N_{BS}} \exp\left[\iota 2\pi p \times \frac{d}{\lambda}\sin(\theta)\cos(\phi)\right] \times \exp\left[\iota 2\pi q \times \frac{d}{\lambda}\sin(\phi)\right] \quad (1)$$

with $\iota = \sqrt{-1}$, horizontal and vertical antenna spacing d, and carrier signal wavelength λ. Here, $d = \lambda/2$ m, i.e., half-wavelength spacing ($2\pi\frac{d}{\lambda} = \pi$), and the DFBS boresight is along the x-axis, i.e., transmit beamformer $\mathbf{f}_{BS} = \mathbf{a}(0^\circ, 0^\circ)$.

The targets are modelled as point scatters with time-invariant channels. For target k with AoA (θ_k,ϕ_k)

$$\mathbf{H}_k = \alpha_k(\sigma_k)\mathbf{a}(\theta_k,\phi_k)\mathbf{a}(\theta_k,\phi_k)^H \in \mathbb{C}^{N_{BS}^2 \times N_{BS}^2} \quad (2)$$

with target radar cross-section (RCS) σ_k. Coefficient $\alpha_k(\sigma_k)$ incorporates complex normal scattering, $\mathcal{CN}(0,\sigma_k^2)$, and two-way pathloss. Pathloss uses frequency and distance dependent terms from a close-in free space reference pathloss model [26].

The DFBS applies beamforming, then transmits the OFDM signal which propagates and reflects from targets. A DFT extracts data symbols from the echoes at each of the N_{BS}^2 antennas. For the ηth subcarrier and μth OFDM time slot [17]

$$\mathbf{d}_{Rx}(\eta,\mu) = d_{Tx}(\eta,\mu)\sum_{k=1}^{K}\mathbf{H}_k\mathbf{f}_{BS}\exp\left[-\iota 2\pi\eta\Delta f\frac{2R_k}{c}\right] \times \exp\left[\iota 2\pi\mu T_{sym} f_{D,k}\right] + \mathbf{z}(\eta,\mu) \quad (3)$$

where $\mathbf{z}$ is additive white Gaussian noise (AWGN) with noise power σ_z^2, i.e., in the pth row and qth column of the UPA, $z(\eta,\mu,p,q) \sim \mathcal{CN}(0,\sigma_z^2)$. Subcarriers, indexed by η, have a linear phase shift dependent on target range $(-2\Delta f R_k/c)$ and OFDM time slots, indexed by μ, have a linear phase shift depending on target velocity $(T_{sym} f_{D,k})$.

III. 4D MMEMP METHOD

A. Matrix enhancement

Received data symbols (3) are compared with transmitted symbols, producing 4D element-wise division tensor, $\mathbf{X}$, with dimension lengths $\mathbf{n} = [N_{ca}, N_{sym}, N_{BS}, N_{BS}]$. For the ηth subcarrier, μth OFDM symbol, and antenna in the pth row and qth column of the UPA

$$x(\eta,\mu,p,q) = \frac{d_{Rx}(\eta,\mu,p,q)}{d_{Tx}(\eta,\mu)} \quad (4)$$

with $d_{Rx}(\eta,\mu,p,q)$ the element (including AWGN) of (3) for this antenna. Phase changes due to range, velocity and angular information, are contained within the data tensor. Sturm and Wiesbeck [6] and our previous works [17], [18] processed (4) with Fourier transforms to estimate the range and velocities of targets. Schmidt's classic MUSIC algorithm [19] searched over azimuth angles [6] or azimuth and elevation angles [17] to estimate target angular information. These methods scan a discrete search space, i.e., are on-grid with large search complexity. We extend the off-grid MMEMP method [15] to estimate target parameters within a 4D parameter space.

Entries in (4) are sums of K 4D sinusoids, $\exp[\iota 2\pi\omega_k(i)]$, with frequencies $\boldsymbol{\omega}_k = [f_{R_k}, f_{v_k}, f_{\theta_k}, f_{\phi_k}]$. Frequencies are normalized, i.e., $f_{R_k} \in [0,1)$ (range is non-negative), $f_{v_k}, f_{\theta_k} \in [-0.5, 0.5)$ and $f_{\phi_k} \in [-0.5, 0)$. The entries are

$$x(\eta,\mu,p,q) = \sum_{k=1}^{K}\beta_k\gamma_{R_k}^{\eta}\gamma_{v_k}^{\mu}\gamma_{\theta_k}^{p}\gamma_{\phi_k}^{q} + z(\eta,\mu,p,q) \quad (5)$$

with β_k complex amplitude, $z(\eta,\mu,p,q)$ AWGN and terms: $\gamma_{R_k} = \exp\left[-\iota 4\pi\Delta f R_k/c\right]$, $\gamma_{v_k} = \exp\left[\iota 2\pi T_{sym} f_{D,k}\right]$, $\gamma_{\theta_k} = \exp\left[\iota\pi\sin(\theta_k)\cos(\phi_k)\right]$, $\gamma_{\phi_k} = \exp\left[\iota\pi\sin(\phi_k)\right]$.

Data tensor $\mathbf{X}$ can then be enhanced to ensure it is full rank. (Block) Hankel matrices are formed by taking moving window segments, with the length of the segments denoted as the 'pencil parameters' $\mathbf{m} = [m_R, m_v, m_\theta, m_\phi]$. In this work $m(i) = \lfloor n(i)/2 \rfloor + 1$, with $\lfloor\cdot\rfloor$ the floor operator and $n(i)$ the length of the corresponding dimension of the data tensor.

Define $\mathcal{H}(\mathbf{A}(i,j,\ldots), m, n)$ as the Hankel operator on tensor $\mathbf{A}$: $[\mathbf{A}(1,j,\ldots), \mathbf{A}(2,j,\ldots), \ldots, \mathbf{A}(m,j,\ldots)]$ is the first column and $[\mathbf{A}(m,j,\ldots), \mathbf{A}(m{+}1,j,\ldots), \ldots, \mathbf{A}(n,j,\ldots)]$ is the last row of the resultant Hankel (block) matrix. The 4D enhanced matrix, $\mathbf{X}_4$, is given by

$$\begin{aligned}
\mathbf{X}_1(\mu,p,q) &= \mathcal{H}(x(\eta,\mu,p,q), m_R, N_{ca}) \\
\mathbf{X}_2(p,q) &= \mathcal{H}(\mathbf{X}_1(\mu,p,q), m_v, N_{sym}) \\
\mathbf{X}_3(q) &= \mathcal{H}(\mathbf{X}_2(p,q), m_\phi, N_{BS}) \\
\mathbf{X}_4 &= \mathcal{H}(\mathbf{X}_3(q), m_\theta, N_{BS})
\end{aligned} \quad (6)$$

where $\mathbf{X}_I$ has $\prod_{i=1}^{I} m(i) \times (n(i) - m(i) + 1)$ elements.

B. Frequency estimation

Estimates of normalized frequencies, $\hat{\boldsymbol{\omega}}_k$, can be extracted from $\mathbf{X}_4$. Singular value decomposition produces

$$\mathbf{X}_4 = \mathbf{U}\mathbf{S}\mathbf{V}^H = \mathbf{U}_s\mathbf{S}_s\mathbf{V}_s^H + \mathbf{U}_z\mathbf{S}_z\mathbf{V}_z^H \quad (7)$$

with $\mathbf{S} \in \mathbb{C}^{\prod\mathbf{m}\times\prod(\mathbf{m}-\mathbf{n}+1)}$ a diagonal matrix of singular values. Columns of $\mathbf{U} \in \mathbb{C}^{\prod\mathbf{m}\times\prod\mathbf{m}}$ and $\mathbf{V} \in \mathbb{C}^{\prod(\mathbf{m}-\mathbf{n}+1)\times\prod(\mathbf{m}-\mathbf{n}+1)}$ are left and right singular vectors.

Subscripts s and z indicate signals or noise respectively, i.e., the first K columns of the parent matrix for signals and remaining columns for noise. K is assumed to be known but can be estimated from $\mathbf{S}$ by thresholding to separate signal-related values and near-zero noise-related values [27].

Define $\bar{m}(i) = \prod_{j\in[1,2,3,4], j\neq i} m(j)$, $\mathcal{U}_1(\mathbf{A}, i)$ as matrix $\mathbf{A}$ with the last $\bar{m}(i)$ rows deleted and $\mathcal{U}_2(\mathbf{A}, i)$ as matrix $\mathbf{A}$ with the first rows $\bar{m}(i)$ deleted. To extract parameters from 4D sinusoids we also define the shuffling matrix, $\mathbf{P}_i \in \mathbb{C}^{\prod\mathbf{m}\times\prod\mathbf{m}}$

$$\begin{aligned}
\mathbf{P}_i = \big[&\mathbf{p}(1);\ \mathbf{p}(1+m(i));\ \ldots\ ;\ \mathbf{p}(1+(\bar{m}(i)-1)m(i)); \\
&\mathbf{p}(2);\ \mathbf{p}(2+m(i));\ \ldots\ ;\ \mathbf{p}(2+(\bar{m}(i)-1)m(i)); \\
&\mathbf{p}(3);\ \ldots\ ;\ \mathbf{p}(m(i)+(\bar{m}(i)-1)m(i))\big]
\end{aligned} \quad (8)$$

where $\mathbf{p}(i) \in \mathbb{C}^{1\times\prod \mathbf{m}}$ is the row vector with a one in its ith position and zero elsewhere.

Poles γ_{ϕ_k} are estimated by generalized eigenvalues (GEs) of matrix pencil $\mathcal{U}_2(\mathbf{U_s}, 4) - \rho\, \mathcal{U}_1(\mathbf{U_s}, 4)$, where $\rho \in \mathbb{C}$. With $\mathbf{A}^\dagger$ the Moore-Penrose pseudoinverse of matrix $\mathbf{A}$ and $\mathrm{diag}(\mathbf{A})$ a diagonal matrix, the eigenvalue decomposition (EVD)

$$\mathrm{diag}(\hat{\gamma}_{\phi_{\tilde{k}}}) = \mathbf{W}^\dagger(\mathcal{U}_\mathbf{1}(\mathbf{U_s}, \mathbf{4})^\dagger \mathcal{U}_2(\mathbf{U_s}, 4))\mathbf{W} \tag{9}$$

yields eigenvectors, $\mathbf{W}$, and GE estimates, $\hat{\gamma}_{\phi_{\tilde{k}}}$, from which $\hat{f}_{\phi_{\tilde{k}}} = \Im(\log(\hat{\gamma}_{\phi_{\tilde{k}}}))/2\pi$ can be extracted and normalized.

The MEMP technique [14] estimates frequencies of the other complex sinusoids from matrix pencils formed by shuffling singular vectors $\mathbf{U}_s$. This results in four sets of unassociated frequencies, requiring a grouping operation to yield a group of estimated frequencies $\hat{\boldsymbol{\omega}}_{\tilde{k}}$ corresponding to one of the K targets. The correlation-based nature of this operation can result in non-associated frequencies being grouped, e.g., giving $\hat{\boldsymbol{\omega}}_k = [\hat{f}_{R_{\tilde{k}}}, \hat{f}_{v_k}, \hat{f}_{\theta_k}, \hat{f}_{\phi_k}]$ with $k \neq \tilde{k}$.

Addressing this, Chen et al. [15] proposed the modified MEMP (MMEMP) technique which simultaneously estimates poles in 2D complex sinusoids, bypassing grouping and attaining similar performance to the MEMP technique. It exploits eigenvectors of the first matrix pencil, $\mathbf{W}$, and is extended to 4D by applying shuffling matrices to $\mathbf{U}_s$

$$\mathrm{diag}(\hat{\gamma}_{R_{\tilde{k}}}) = \mathbf{W}^\dagger(\mathcal{U}_1(\mathbf{P}_1\mathbf{U_s}, 1)^\dagger \mathcal{U}_2(\mathbf{P}_1\mathbf{U_s}, 1))\mathbf{W} \tag{10}$$

$$\mathrm{diag}(\hat{\gamma}_{v_{\tilde{k}}}) = \mathbf{W}^\dagger(\mathcal{U}_1(\mathbf{P}_{21}\mathbf{U_s}, 2)^\dagger \mathcal{U}_2(\mathbf{P}_{21}\mathbf{U_s}, 2))\mathbf{W} \tag{11}$$

$$\mathrm{diag}(\hat{\gamma}_{\theta_{\tilde{k}}}) = \mathbf{W}^\dagger(\mathcal{U}_1(\mathbf{P}_{321}\mathbf{U_s}, 3)^\dagger \mathcal{U}_2(\mathbf{P}_{321}\mathbf{U_s}, 3))\mathbf{W} \tag{12}$$

with $\mathbf{P}_{21} = \mathbf{P}_2\mathbf{P}_1$ and $\mathbf{P}_{321} = \mathbf{P}_3\mathbf{P}_{21}$. Frequencies in the same $\tilde{k}$th diagonal position correspond to the same target, allowing estimation of target parameters $\hat{\mathbf{w}}_{\tilde{k}} = [\hat{R}_{\tilde{k}}, \hat{v}_{\tilde{k}}, \hat{\theta}_{\tilde{k}}, \hat{\phi}_{\tilde{k}}]$.

Equations (9)-(12) provide solutions for the case where each of parameters are distinct between targets. When multiple targets share, e.g. the same range, the MMEMP technique can still be applied by extracting non-diagonal block matrices from the initial solutions of (9)-(12) and performing additional EVDs. Treatment is not provided here due to space constraints but it has been given in 2D [15] and 3D [16].

To assess performance, the 4D 2-norm distances $||\boldsymbol{\omega}_k - \hat{\boldsymbol{\omega}}_{\tilde{k}}||$ for $k, \tilde{k} = 1, \ldots, K$, were used to match group estimates to targets by smallest distance to largest, with each group corresponding to a unique target. This prioritized achieving the best possible estimate for one of the targets, rather than minimizing a global error between estimate-target matches.

C. Cramér-Rao lower bound

The Cramér-Rao lower bound (CRLB) is a lower bound on the variance of the unbiased estimation of the target parameters from noisy data [25]. Unknown parameters are given in the vector $\boldsymbol{\nu} = [\boldsymbol{\nu}_1; \boldsymbol{\nu}_2; \ldots; \boldsymbol{\nu}_K] \in \mathbb{C}^{6K\times1}$ with

$$\boldsymbol{\nu}_k = [|\beta_k|;\ \angle\beta_k;\ R_k;\ v_k;\ \theta_k;\ \phi_k] \in \mathbb{C}^{6\times1} \tag{13}$$

where $|\beta_k|$ and $\angle\beta_k$ are the magnitude and phase of β_k.

To calculate the CRLB of each parameter, the Fisher Information Matrix (FIM), $\mathbf{F} \in \mathbb{C}^{6K\times6K}$, must be calculated. The FIM is made of block matrices $\mathbf{F}_{ab} \in \mathbb{C}^{6\times6}$, where a is the row and b the column of this block in the FIM. The entry of the ith row and jth column in this block is

$$F_{ab}(i,j) = \frac{2}{\sigma_z^2}\Re\left(\frac{\partial\mathbf{x}^H}{\partial\nu_a(i)}\frac{\partial\mathbf{x}}{\partial\nu_b(j)}\right) \tag{14}$$

with σ_z^2 the noise power and $\mathbf{x}$ is the vector of entries in (5) without inclusion of the AWGN, $\mathbf{z}$.

From differentiation with respect to angle parameters, θ_k and ϕ_k, entries in the FIM contain summations of trigonometric functions with phases dependent on the differences between (θ_a, ϕ_a) and (θ_b, ϕ_b). Analytical expressions for the FIM are not included here due to space constraints.

The CRLB for the variance of the normalized frequency estimates in $\boldsymbol{\nu}$ are diagonal elements of the inverse of the FIM, $\mathbf{F}^{-1}$. For the UPA, the CRLB for θ_k and ϕ_k are independent of one another [28].

IV. Simulation Results

In Fifth Generation New Radio (5G NR) standards the 'numerology', μ_{5G}, determines suitable carrier frequencies, subcarrier spacing, $\Delta f = 15 \times 2^{\mu_{5G}}$ kHz, and OFDM time slot length, $T_{sym} = 1000/(14 \times 2^{\mu_{5G}})$ μs [29]. In our simulations we set carrier frequency $f_c = 6$ GHz and $\mu_{5G} = 0$ ($\Delta f = 15$ kHz, $T_{sym} = 71.42$ μs). Target parameters are within limits, $R_k \in [0, c/(2\Delta f)), v_k \in [-c/(4T_{sym}f_c), +c/(4T_{sym}f_c)), \theta_k \in [-\pi/2, \pi/2)$ and $\phi_k \in [-\pi/2, 0)$. Data tensor dimensions $\mathbf{n}$, pencil parameters $\mathbf{m}$, and size of enhanced matrix $\mathbf{X}_4$ are changed by varying the number of data subcarriers, OFDM symbols and number of antennas. We demonstrate simulations with equally sized data tensor dimensions $n(i) = n$ for $i = 1, \ldots, 4$, denoted n^4. Methodology and shuffling matrices provided can be applied to data tensors with differently sized dimensions. Data is encoded into 4-QAM symbols. The UPA boresight is along the x-axis.

Point targets each have an RCS of 1 m^2 and parameters $\mathbf{w}_1 = [4300\text{ m}, -20\text{ m/s}, -10°, -70°]$, $\mathbf{w}_2 = [4600\text{ m}, 10\text{ m/s}, 30°, -35°]$, and $\mathbf{w}_3 = [4900\text{ m}, 30\text{ m/s}, 50°, -20°]$, respecting constraints related to Doppler shift and guard period. Due to DFBS beamforming, random reflection coefficients and pathloss, the targets have different effective gains for received signal powers of $[-2.98, 0, -20.88]$ dB respectively, relative to target two. When simulated individually, the effective gain 0 dB as noise power at each antenna is defined relative to the received signal power and SNR, $\sigma_z^2 = P_{Rx} \times 10^{-\mathrm{SNR}/10}$, where P_{Rx} is received signal power without noise in watts. The results presented are the average of $1,000$ realizations of the simulations with random noise.

Performance of the 4D MMEMP technique is demonstrated by giving the mean-squared errors (MSE) against SNR for estimates of each of the four parameters of a single target with parameters $\mathbf{w}_1$. The 4D MMEMP technique is applied to data tensors with sizes 4^4, 6^4, 8^4 and 10^4. In Fig. 1 (and Fig. 2) the solid colored lines represent MSE and dashed lines of the same color give the CRLB for that data tensor size.

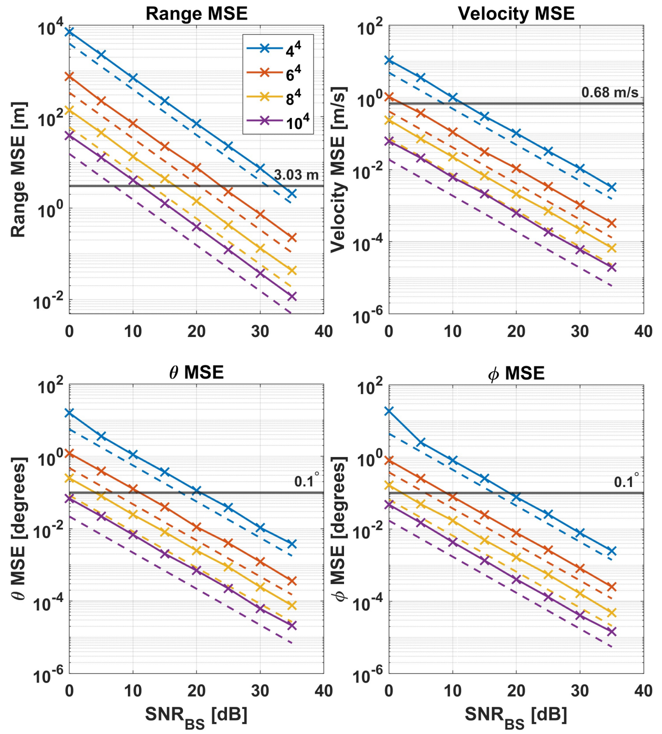

Fig. 1. Parameter estimation for one target with $\mathbf{X} \in \mathbb{C}^{4^4}, \mathbb{C}^{6^4}, \mathbb{C}^{8^4}, \mathbb{C}^{10^4}$.

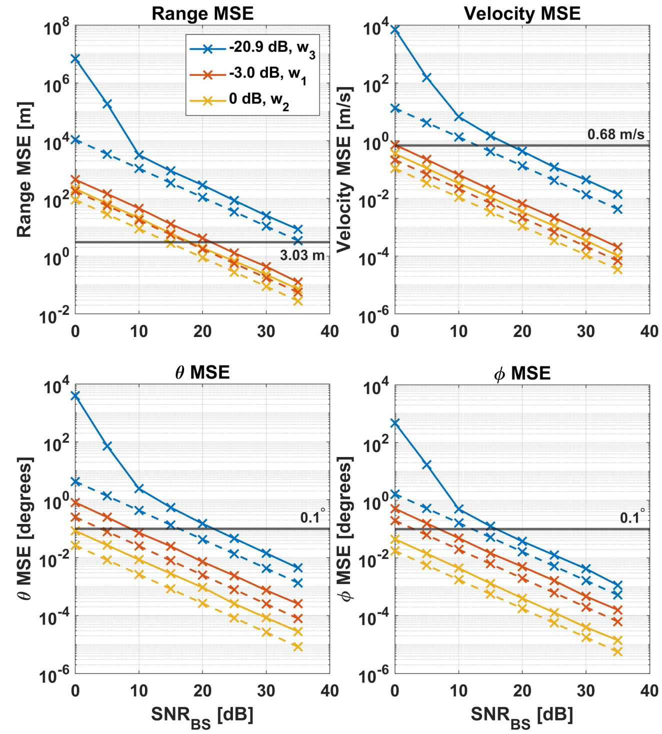

Fig. 2. Parameter estimation for three targets of different gains and $\mathbf{X} \in \mathbb{C}^{8^4}$.

The MSE linearly reduce with increasing SNR, whereas an increase in n^4 reduces MSE nonlinearly. Diminishing returns for increasing the data tensor size are seen: increasing the data tensor size from 4^4 to 6^4 is equivalent to a 10 dB increase in SNR but an increase from 8^4 to 10^4 is only equivalent to a 5 dB SNR improvement. MSE of estimates for target parameters are close to the CRLBs, but there is a slight trend for the gap between MSE and the CRLBs to increase with increasing n^4. The parameter estimate MSE are not the same, due to scaling between the estimates of frequencies, $\hat{\boldsymbol{\omega}}_k$, and corresponding parameters, $\hat{\mathbf{w}}_k$. MSE for the range estimates are large as small errors in $\hat{f}_{R_k}$ scale to large $\hat{R}_k$ errors. This could be compensated by increasing the size of the corresponding data tensor dimension, i.e., number of subcarriers.

In this figure the black lines represent the resolutions of parameter estimates using the Fourier-based and MUSIC algorithm. Resolutions for Fourier technique estimates of range and velocity are given from a system using a large number of data subcarriers and OFDM symbols as in [17], with resulting resolutions of 3.03 m for range and 0.68 m/s for velocity with $N_{ca} = 3300$ and $N_{sym} = 512$. The 4D MMEMP-based estimation of velocity is more precise than Fourier-based estimation for nearly all SNRs and data tensor sizes. However, due to frequency-parameter scaling, to outperform the Fourier technique on range estimates the 4D MMEMP technique requires a high SNR (20+ dB) and a large data tensor size (large number of subcarriers). In comparison to a fine $0.1°$ search resolution possible with the MUSIC algorithm, the 4D MMEMP technique is more precise at nearly all SNRs and data tensor sizes.

In Fig. 2 we present MSE for parameter estimates for data tensor size 8^4 in a scenario with $K = 3$ targets with parameters, $\mathbf{w}_1, \mathbf{w}_2$ and $\mathbf{w}_3$. With increasing SNR the MSE reduce for all targets and targets with weaker reflections have higher MSE. At low SNRs $(0, 5$ dB) the echo from target three is so weak, relative to noise, that the parameters cannot be estimated reliably, taking random values within the search limits. The MSE for θ_3 at low SNRs are higher than for ϕ_3 as the search space is doubled, i.e., $f_{\theta_k} \in [-0.5, 0.5)$ and $f_{\phi_k} \in [-0.5, 0) \ \forall \ k$. The other targets, with stronger echoes, are reliably estimated. Black lines are the same as in Fig. 1.

V. Conclusions

We have simulated a 5G NR-compliant OFDM-based DFCR system, extending the MMEMP method to perform parameter estimation in 4D, using MSE as a performance metric. Range, velocity, azimuth angle and elevation angles have been estimated for multiple point targets in a scenario.

It has been shown that the target parameters can be accurately and precisely estimated with the 4D MMEMP technique with large data tensor sizes and when the SNR is high. The 4D MMEMP technique is off-grid and so can attain higher precision estimates than Fourier-based or MUSIC techniques. Its performance is close to that of the CRLB.

When the SNR is low a high precision estimate can be obtained by processing a large data tensor: similarly, high SNRs can compensate reduction in precision for small data tensors. For more precise estimates of a specific parameter, the corresponding dimension of the data tensor can be increased.

REFERENCES

[1] Ericsson, "Ericsson mobility report," Ericcson, Tech. Rep., November 2022.

[2] F. Liu, C. Masouros, A. P. Petropulu, H. Griffiths, and L. Hanzo, "Joint radar and communication design: Applications, state-of-the-art, and the road ahead," *IEEE Transactions on Communications*, vol. 68, no. 6, pp. 3834–3862, 2020.

[3] A. Schlegel, W. R. Torres, and J. A. Nanzer, "Joint sensing and communication via superposition of spectrally-sparse radar and BPSK signals," in *Proc. of 2022 IEEE International Symposium on Antennas and Propagation and USNC-URSI Radio Science Meeting (AP-S/URSI)*, Denver, CO, USA, 2022, pp. 531–532.

[4] J. Zhang, N. Garg, and T. Ratnarajah, "In-band-full-duplex integrated sensing and communications for IAB networks," *IEEE Transactions on Vehicular Technology*, vol. 71, no. 12, pp. 12 782–12 796, 2022.

[5] C. Sturm, T. Zwick, and W. Wiesbeck, "An OFDM system concept for joint radar and communications operations," in *Proc. of 2009 IEEE 69th Vehicular Technology Conference (VTC)*, Barcelona, Spain, 2009, pp. 1–5.

[6] C. Sturm and W. Wiesbeck, "Waveform design and signal processing aspects for fusion of wireless communications and radar sensing," *Proceedings of the IEEE*, vol. 99, no. 7, pp. 1236–1259, 2011.

[7] Y. Hua and T. Sarkar, "Matrix pencil method for estimating parameters of exponentially damped/undamped sinusoids in noise," *IEEE Transactions on Acoustics, Speech, and Signal Processing*, vol. 38, no. 5, pp. 814–824, 1990.

[8] L. Monteyne, A. P. Guevara, G. Callebaut, S. Gunnarsson, L. Van der Perre, and S. Pollin, "Matrix pencil method: Angle of arrival and channel estimation for a massive MIMO system," in *Proc. of 2020 IEEE International Conference on Communications (ICC)*, Dublin, Ireland, 2020, pp. 1–6.

[9] X. Ma, Z. Zhou, K. Liu, J. Zhang, and W. Raza, "Poles extraction of underwater targets based on matrix pencil method," *IEEE Access*, vol. 8, pp. 103 007–103 019, 2020.

[10] A. Bazzi, D. T. M. Slock, and L. Meilhac, "Single snapshot joint estimation of angles and times of arrival: A 2D matrix pencil approach," in *Proc. of 2016 IEEE International Conference on Communications (ICC)*, Kuala Lumpur, Malaysia, 2016, pp. 1–6.

[11] Y. Zheng and Y. Yu, "Joint estimation of DOA and TDOA of multiple reflections by matrix pencil in mobile communications," *IEEE Access*, vol. 7, pp. 15 469–15 477, 2019.

[12] B. Ji, Y. Wang, B. Zhao, X. Lu, and R. Xu, "Novel super-resolution ISAR imaging method via two-dimensional unitary matrix pencil algorithm," in *Proc. of 2020 15th IEEE International Conference on Signal Processing (ICSP)*, Beijing, China, 2020, pp. 600–604.

[13] N. Yilmazer, R. Fernandez-Recio, and T. K. Sarkar, "Matrix pencil method for simultaneously estimating azimuth and elevation angles of arrival along with the frequency of the incoming signals," *Digital Signal Processing*, vol. 16, no. 6, pp. 796–816, 2006.

[14] Y. Hua, "Estimating two-dimensional frequencies by matrix enhancement and matrix pencil," *IEEE Transactions on Signal Processing*, vol. 40, no. 9, pp. 2267–2280, 1992.

[15] F.-J. Chen, C. C. Fung, C.-W. Kok, and S. Kwong, "Estimation of two-dimensional frequencies using modified matrix pencil method," *IEEE Transactions on Signal Processing*, vol. 55, no. 2, pp. 718–724, 2007.

[16] M. F. Khan and M. A. Tufail, "Simultaneous estimation of azimuth and elevation angles and frequency of plane wave signals using a modified matrix pencil method," in *Proc. of 2008 23rd International Technical Conference on Circuits/Systems, Computers and Communications (ITC-CSCC)*, Shimonoseki City, Yamaguchi, Japan, 2008, pp. 873–876.

[17] S. P. Lavery and T. Ratnarajah, "Airborne phased array OFDM joint radar-communications system," in *Proc. of 2022 IEEE Radar Conference (RadarConf22)*, New York City, NY, USA, 2022, pp. 1–6.

[18] ——, "Airborne OFDM joint communications-radar system for observing extended targets," in *Proc. of International Conference on Radar Systems (RADAR 2022)*, Edinburgh, UK, 2022, pp. 347–352.

[19] R. Schmidt, "Multiple emitter location and signal parameter estimation," *IEEE Transactions on Antennas and Propagation*, vol. 34, no. 3, pp. 276–280, 1986.

[20] S. Ahmed, T. Ratnarajah, M. Sellathurai, and C. F. N. Cowan, "Iterative receivers for MIMO-OFDM and their convergence behavior," *IEEE Transactions on Vehicular Technology*, vol. 58, no. 1, pp. 461–468, 2009.

[21] C. B. Barneto, T. Riihonen, M. Turunen, L. Anttila, M. Fleischer, K. Stadius, J. Ryynänen, and M. Valkama, "Full-duplex OFDM radar with LTE and 5G NR waveforms: Challenges, solutions, and measurements," *IEEE Transactions on Microwave Theory and Techniques*, vol. 67, no. 10, pp. 4042–4054, 2019.

[22] H. Luo, M. Holm, and T. Ratnarajah, "On the performance of active analog self-interference cancellation techniques for beyond 5G systems," *China Communications*, vol. 18, no. 10, pp. 158–168, 2021.

[23] Y. Hou, S. Cai, W. Xia, J. Zhang, and S. Xia, "Self-interference cancellation based on symbol-level precoding for dual-function radar and communication systems," in *Proc. of 2022 IEEE/CIC International Conference on Communications in China (ICCC Workshops)*, Foshan City, China, 2022, pp. 140–145.

[24] D. Roque and S. Bidon, "Range migration in symbol-based OFDM radar receivers," in *Proc. of 2021 IEEE 22nd International Workshop on Signal Processing Advances in Wireless Communications (SPAWC)*, Lucca, Italy, 2021, pp. 496–500.

[25] H. L. V. Trees, *Optimum Array Processing: Part IV of Detection, Estimation, and Modulation Theory*. New York City, NY, USA: John Wiley & Sons, Inc., 2002.

[26] S. Sun, G. R. MacCartney, and T. S. Rappaport, "A novel millimeter-wave channel simulator and applications for 5G wireless communications," in *Proc. of 2017 IEEE International Conference on Communications (ICC)*, Paris, France, 2017, pp. 1–7.

[27] K. Konstantinides and K. Yao, "Statistical analysis of effective singular values in matrix rank determination," *IEEE Transactions on Acoustics, Speech, and Signal Processing*, vol. 36, no. 5, pp. 757–763, 1988.

[28] R. Nielsen, "Azimuth and elevation angle estimation with a three-dimensional array," *IEEE Journal of Oceanic Engineering*, vol. 19, no. 1, pp. 84–86, 1994.

[29] 3GPP, "Release 15 description; summary of Rel-15 work items," 3rd Generation Partnership Project (3GPP), Technical Specification (TS) 21.195, 2019, version 15.0.0.